


# Quantifying Turbidity Variation for Lakes in Daqing of Northeast China Using Landsat Images From 1984 to 2018

Xiaodi Wang, Kaishan Song , Zhidan Wen , Ge Liu, Yingxin Shang, Chong Fang, Lili Lyu, and Qiang Wang

**Abstract**—Water turbidity is an important proxy to measure water quality and environmental conditions. Based on extensive field data and Landsat data (2011–2018), this article developed a retrieval model suitable for turbidity. The determination coefficient ( $R^2$ ) of the model was 0.946 and the root-mean-square error was 23.82 NTU. The model was implemented to obtain the turbidity information of hundreds of lakes in Northeast China (1984–2018). The results revealed the distinctive spatial pattern of water turbidity values of the lakes (i.e., high turbidity in the south; low turbidity in the northwest; and moderate turbidity in the east). In terms of temporal pattern, the water turbidity values of most lakes trended downward at an average rate of 1.39 NTU/a ( $P < 0.05$ ) with obvious seasonal differences (i.e., decreased from May to the lowest in July, and then increased from September onward). Finally, we quantitatively examined how several typical factors affect turbidity variation at different scales. We found that water turbidity was highly correlated with NDVI ( $R = 0.56, P < 0.001$ ), followed by water temperature and wind speed ( $0.02 < R < 0.5, P < 0.05$ ). Water turbidity varies because of the interaction of multiple factors (e.g., area, temperature, water depth, precipitation, and land use) instead of one factor. This article highlights the potential of remote sensing in large-scale and long-term monitoring of lake water quality, and provides important information and support for water quality management in China.

**Index Terms**—Long-term change, satellite remote sensing, turbidity, vegetation coverage.

## I. INTRODUCTION

**L**AKES are one of the most important components of the earth's surface system [1]–[3]. Lakes provide a main source

Manuscript received April 12, 2021; revised June 12, 2021 and July 19, 2021; accepted July 27, 2021. Date of publication August 4, 2021; date of current version September 15, 2021. This work was supported by the program and the National Natural Science Foundation of China under Grants 41730104, 42071336, and 41771067. The work of K. Song and Z. Wen was supported by the Natural Science Foundation of Heilongjiang Province under Grants LH2019D010, ZD2020D002, and D2018007. (Corresponding author: Kaishan Song.)

Xiaodi Wang is with the Northeast Institute of Geography and Agroecology, Chinese Academy of Sciences, Changchun 130102, China, and also with Harbin University, Harbin 150086, China (e-mail: yayawxd123@126.com).

Kaishan Song is with the Northeast Institute of Geography and Agroecology, Chinese Academy of Sciences, Changchun 130102, China, and also with the School of Environment and Planning, Liaocheng University, Liaocheng 252000, China (e-mail: songkaishan@iga.ac.cn).

Zhidan Wen, Ge Liu, Yingxin Shang, Chong Fang, Lili Lyu, and Qiang Wang are with the Northeast Institute of Geography and Agroecology, Chinese Academy of Sciences, Changchun 130102, China (e-mail: wenzhidan@iga.ac.cn; liuge@iga.ac.cn; shangyingxin@iga.ac.cn; fangchong@dlut.edu.cn; lvlili@iga.ac.cn; 15590287488@163.com).

Digital Object Identifier 10.1109/JSTARS.2021.3101475

of potable water; serve various functions, such as irrigation, aquaculture, storage and regulation, tourism and ecological balance; and play an important role in regional, ecosystems and global biogeochemical cycles [4], [5]. These important effects are especially evident in Daqing Lakes, the largest lake gathering place in Northeast China [6], [7]. The water quality of lakes can directly influence the survival of human beings and sustainable development of society [8]. However, many lakes are encountering water quality problems because of rapid urbanization, industrialization, agricultural intensification, anthropogenic interference and climate change [9], [10]. To improve water quality management, and sustainability of water safety, there is an urgent need for quantification of water quality and water pollution degree [11], [12]. Turbidity is an important indicator of the water quality and environmental safety of lakes [13], [14]. Turbidity can effectively reflect the ecohydrological processes and light efficiency of lake and reservoir ecosystem; directly affect the attenuation of light in water body and alter the primary productivity of water body [15], [16]. The assessment of water turbidity is a key issue in environmental monitoring and management [17], [18]. Therefore, the timely and accurate estimation of turbidity in waters is essential to better understand the water quality; determine the drivers that influence turbidity; and support efficient management [11], [19].

Traditionally, turbidity information has been collected primarily through field measurement and experimental analysis [20], [21]. However, using traditional methods to estimate turbidity requires a great deal of materials, time, and human resources; and it is difficult to obtain spatiotemporal patterns [18]. Remote sensing data contain the characteristics of wide spatiotemporal coverage and low cost. Especially, water quality remote sensing information is usually used as an important basis for lake monitoring, which has attracted great interest and wide attention of research community [22], [23]. However, it is more feasible to retrieve turbidity using remote sensing [24], [25]. Many studies have applied optical remote sensing technique to estimate various water quality parameters e.g., total suspended matter, chlorophyll A, N/P and water depth [26], [27]. However, few studies examined, the application of remote sensing in turbidity inversion. Besides, the existing knowledge about the spatiotemporal dynamics of water turbidity over long time span and high spatial resolution is poor [28], [29].

In recent years, the advantages of remote sensing data in water resources research are becoming more obvious [30], [31].

Various remote sensing data with different spatial resolutions and spectral bands have been utilized for estimating water turbidity, such as Landsat, sea-viewing wide field-of-view sensor (SeaWiFS), medium resolution imaging spectrometer, and moderate resolution imaging spectrometer [11], [32]. In this sense, satellite remote sensing plays an important role in monitoring the spatiotemporal dynamics water turbidity and maintaining the sustainable development of water environment [33], [34].

Relative to other remote sensing data, Landsat images contain a higher spatiotemporal resolution. This can assist the analysis of long-term historical evolution, and support the estimation of the spatial and temporal variations of water turbidity [11]. Some previous studies have made preliminary analysis and discussion about the turbidity of coastal waters using remote sensing data [35]. Nevertheless, the sensitive bands of satellite sensors are different for different types of water bodies [36], [37]. To accurately retrieve turbidity information from lake water, a band with sufficient sensitivity is required. At present, the turbidity inversion model based on Landsat is incomplete because of the complex optical properties of turbidity. In addition, the turbidity in inland waters could be greatly affected by climate change and anthropogenic activities [38], [39]. Thus, it is essential to combine remote sensing images with measured data in order to estimate the spatial and temporal patterns of turbidity in inland waters.

Daqing city is the largest lake gathering place in Northeast China and one of the top ten petroleum cities in China [40]. These densely distributed lakes in or around Daqing city are collectively called the Daqing lakes in this article. At the same time, Songnen Plain, where the lakes are located, is an important grain production base in China [41]–[43]. Therefore, the Daqing lakes play an important role in providing drinking water, industrial and agricultural water, and domestic water for local residents. The inland lakes of Daqing are densely distributed, which is a typical region with intensive human activities, such as industrial and agricultural development in Northeast China [44]. Du *et al.* estimated the spatial and temporal pattern of TSM in Northeast China and found that TSM showed a decreasing trend year by year. Since TSM is an important cause of water turbidity, we assume that the water turbidity in this article area will also present similar characteristics of time variation, which will be further verified in this article. In addition, the water bodies of Daqing lakes are also more sensitive to climate change [45]. However, existing studies primarily focused on the recent hydrological changes of inland lakes based on quantitative analysis of remote sensing data [11], [46]. There are limited studies about the long-term (e.g., annual and monthly) spatiotemporal patterns of water turbidity in Daqing lakes under climate change and anthropogenic intensive human activities. There is a lack of systematic and comprehensive analysis on the long-term continuous change of turbidity and its potential driving factors.

This article has three key objectives.

- 1) We verify the advantages of Landsat remote sensing data and Acolite (atmospheric correction for OLI “lite”) method in estimating the spatiotemporal variation of long-term turbidity and retrieve the turbidity in the inland lakes of the study area.

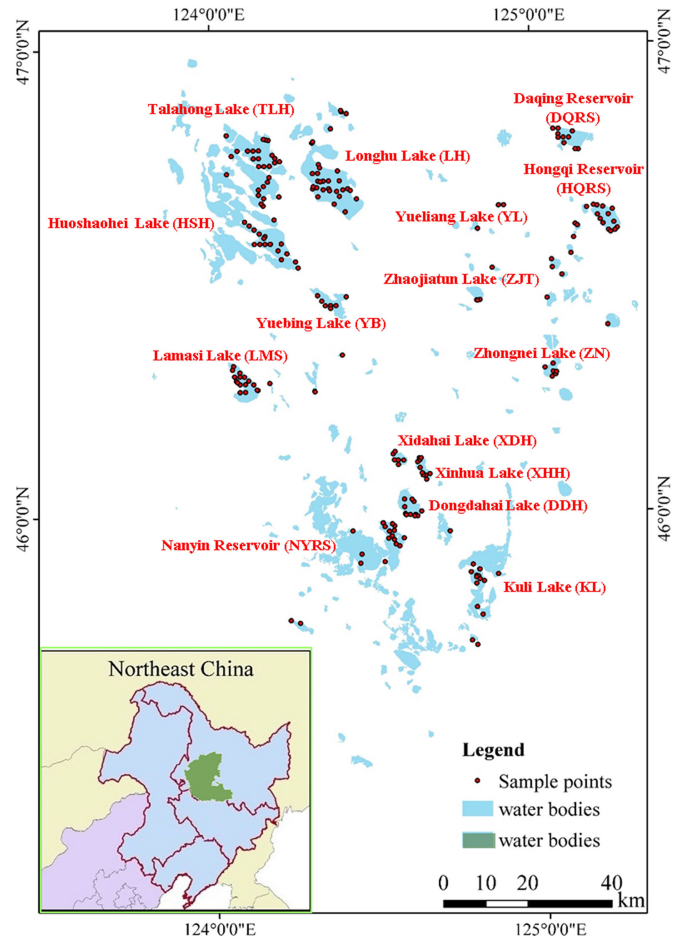


Fig. 1. Spatial distribution of sample points and typical lakes in study area.

- 2) We mapped the spatiotemporal dynamics pattern of turbidity across the study area using the robust model for identifying the areas of persistently elevated turbidity (which might experience serious water quality issues).
- 3) The correlations between turbidity variations and factors were explored for the implementation of water quality management.

## II. MATERIALS AND METHODS

### A. Study Area

The Daqing lakes are located in the north of Songnen Plain and on the left bank of Nenjiang River, China ( $124^{\circ}19'48'' \sim 125^{\circ}12'6''$  E,  $45^{\circ}46'18'' \sim 46^{\circ}55'54''$  N). It is the largest lake cluster in Songnen Plain [45]. The lakes are mainly located in Daqing city, the largest oil production base in China (see Fig. 1). Daqing lakes belong to the north temperate subhumid continental monsoon climate zone, with an annual average temperature of  $4.2^{\circ}\text{C}$ . The annual average precipitation is 427.5 mm, and the annual average evaporation is 1635 mm. The rainy season of the Daqing lakes is mainly concentrated in July and August, and 55–80% of the annual precipitation is concentrated in June–September, which may cause drought and severe water shortage in April–June [47]. The Daqing lakes are an important source of water for industry and agriculture in Heilongjiang

Province of China; and an important source of drinking water for urban residents, providing more than 90 % of the drinking water for more than 3 million urban residents [48]. The total wetland area of Daqing lakes is about 18 580 km<sup>2</sup>, and the Daqing lakes include hundreds of large or small lakes [49]. The lake area is about 1196.34 km<sup>2</sup> (approximately 7% of the total wetland area); and the water depth varies from 1 to 7 m. Since the exploitation of Daqing Oil Field in 1959, the population and construction land area of Daqing city have been rising, followed by increasing domestic sewage and industrial wastewater discharge, shrinking lake area, declining water quality and other environmental problems [44]. Serious eutrophication and fish death in some of the lakes are affecting human safety and aquatic ecosystem.

### B. Field Survey and Sampling Design

From 2011 to 2018, a total of 218 water samples were collected from 23 lakes of the Daqing Lakes. The number of sampling points of each lake was determined by the lake area. In general, we set 8–15 sampling points for a large lake ( $\geq 10$  km<sup>2</sup>) and 3–8 sampling points for a small lake ( $< 10$  km<sup>2</sup>). Fig. 1 displays the spatial distribution of sampling points of the Daqing lakes in Northeast China. According to different geographical locations, lake areas and types, we selected 15 typical lakes uniformly distributed in Daqing for analysis and discussion. Among these lakes, Huoshaohei (HSH), Lamasi, Talahong (TLH) and Yuebing lakes with larger area and deeper water are located in the northwest of Daqing Lakes and used for agricultural irrigation. Xinhua, Xidahai (XDH), and Dongdahai (DDH) lakes are all small and shallow lakes distributed in the south of Daqing Lakes and nearby large factories. Nanyin Reservoir and Kuli Lake (KL) lakes are typical agricultural irrigation lakes distributed in the southern part of Daqing Lakes. Zhaojiatun (ZJT), Zhongnei (ZN), Yueliang (YL), and other lakes are all located in the east of Daqing Lakes and near the city center and residential areas. They are typical urban lakes. Daqing reservoir (DQRS), Hongqi Reservoir (HQRS), and Longhu (LH) lakes are the important sources of potable water for residents of Daqing.

During field survey, each water sample was collected from 0.5 m below water surface using a picking polyethylene sample bottle. Subsequently, the water samples were stored in coolers (with ice packs) and transported to the Remote Sensing Laboratory of Water Environment (Changchun, China) within 18–24 h. The turbidity of each water sample was measured in the laboratory using the photometric method (see detailed description in Constantin *et al.* [50]).

### C. Landsat Imagery Data

1) *Imagery Selection:* Imagery data were selected in accordance to the Landsat overpasses with respect to the specific dates of field surveys conducted during 2011–2018. Kloiber *et al.* and Song *et al.* suggested that simultaneous image acquisition within three days would improve the simulation effect of turbidity remote sensing model [51], [52]. However, Landsat revisits every 16 days, thus it is difficult to ensure the satellite transit time to be consistent with field survey time. Therefore, this article assumed that the water turbidity was relatively stable, and the time

window of Landsat crossing was broadened to  $\pm 10$  days [53], [54]. To minimize the interference of clouds on Landsat images and turbidity estimation, only images with cloud cover  $< 5\%$  were used in this article [55]. After considering the characteristics of ice and snow cover during winter in Northeast China, this article merely applied Landsat images from May to October during 2011–2018. Eventually, we downloaded 10 Landsat images with synchronous turbidity samples ( $\leq 10$  days) from the U.S. Geological Survey (USGS) website.<sup>1</sup>

2) *Atmospheric Correction and Performance Evaluation:* Landsat images covering the study region from 1984 to 2018 (TM: Thematic mapper instruments, ETM: Enhanced Thematic mapper plus scanner, and OLI: Operational land imager) were applied for turbidity retrieval. All optical remote sensing images without cloud cover were processed using SeaDAS software to produce the Rayleigh-corrected reflectance (Rrc). We obtained four types of reflectivity products from Landsat images and processed them as follows. The first reflectance product is the calibrated top of atmosphere (TOA) reflectance [denoted as  $\rho(\lambda)$ ], which does not eliminate the aerosol scattering and Rayleigh scattering effects on satellite signals after atmospheric correction [56]. The second reflectivity product is the surface reflectance science product  $R_s(\lambda)$ , which eliminates the aerosol scattering and Rayleigh scattering effects on satellite signals after atmospheric correction [57]. The third reflectivity product  $R_{\text{hot}}(\lambda)$  is the Rayleigh corrected reflectivity [58], [59], which removes the effects of Rayleigh (molecular) scattering, leaving the effects of aerosols. The fourth product is  $R_{\text{rs}}(\lambda)$  obtained using the Acolite Python software and the “dark spectral fitting” atmospheric correction method [60]. We also applied the ASD spectrometer to resample the in-situ measured spectra of 218 samples, and made relative correction for the reflectance of satellite remote sensing images. The product we finally chose was the  $R_{\text{hot}}$ , because the estimated turbidity values of  $R_{\text{rs}}$  and other products all had many negative values, which did not conform to the real data results of turbidity. This may be because  $R_{\text{rs}}$  and other products are more suitable for Marine water bodies, while  $R_{\text{hot}}$  product is more suitable for secondary inland water bodies, especially for lake water bodies with high turbidity [61]. Therefore, the estimation results of turbidity inversion based on  $R_{\text{hot}}$  products are selected in this article. Finally, we used Landsat images for the turbidity inversion mapping of Daqing lakes. It has been verified that the turbidity estimation retrieved from  $R_{\text{hot}}$  products has a high accuracy of up to 90%.

### D. Water Body Mask Preparation

The spectral characteristics of a water body are different from those of a land surface [62]. With the increase of the wavelength from the visible band to the near-infrared band, the spectral reflectance of water gradually decreases and reaches the lowest level in the near-infrared band [60]. Some studies extracted water bodies using the automatic extraction method of enhancing the contrast of visible and near-infrared bands [e.g.,

<sup>1</sup>[Online]. Available: <http://glovis.usgs.gov/>

NDVI (Defries and Townshend, 1994) and normalized differential water index (NDWI) (McFeeters, 1996)] and obtained better extraction results [61], [62]. In this article, we used band ratios (green/SWIR or green/NIR), normalized difference water index (NDWI), tasseled cap transformation (TC), and a density slicing with multi-threshold approach based on decision tree to distinguish water and nonwater area [63]. Then, Arcgis10.3 software was used to convert the extracted water into polygons with continuous pixels, which were stored in a shape file. Here, water bodies with an area of less than 0.5 km<sup>2</sup> were excluded [11]. However, automatic extraction of lake area cannot fully and effectively solve the problem of mixed pixels along the lake boundary. Besides, the identified water body may contain other redundant elements, such as surrounding floodplains or rivers. Hence, we manually modified the extracted lake boundary to refine the identification accuracy [52]. The lake shape file was further used as the water mask to extract the turbidity map derived from the Landsat imagery data.

### E. Model Calibration and Validation

All possible light band values and band combinations (such as addition, subtraction, multiplication, ratio, and average) were calculated. The Pearson correlation analysis was performed for these bands/band combinations and turbidity to compare and determine the most sensitive bands or band combinations of turbidity. On this basis, the empirical models of turbidity value and remote sensing data of 158 samples were established. The remaining 60 samples were used for validation. The independent variables were Landsat bands/band combinations and the dependent variable was the turbidity. To evaluate the accuracy of the turbidity inversion model, the determination coefficient ( $R^2$ ) and root-mean-square error (RMSE) were used. The RMSE was calculated using (Yang *et al.*, 2020)

$$RMSE = \sqrt{\frac{\sum_{i=1}^n (X_{Est} - X_{obs})^2}{n}} \quad (1)$$

where  $X_{Est}$  and  $X_{obs}$  are the simulated and measured values, respectively; and  $n$  is the number of samples.

After developing the regression model, Landsat images from 1984 to 2018 were used to predict the turbidity of the study area. Then, the annual mean turbidity value of the whole study area was calculated. At the same time, yearly and monthly turbidity values were also calculated for the whole study area and 15 typical lakes.

## III. RESULTS

### A. Landsat-Based Models for Turbidity

The correlation analysis results (see Fig. 2) show strong correlations between some band combinations (e.g., (Blue+NIR)\*NIR, Blue\*Green\*NIR, Green\*Red\*NIR, (Red+NIR)\*(Blue+NIR), Red\*NIR, (Blue+Red)\*NIR, (Blue+Green)\*NIR, (Green+NIR)\*(Blue+NIR), and Blue\*NIR) and turbidity. Their correlation coefficients ranged from 0.92 to 0.95. These nine optimal band combinations were selected to establish fitting empirical models with measured

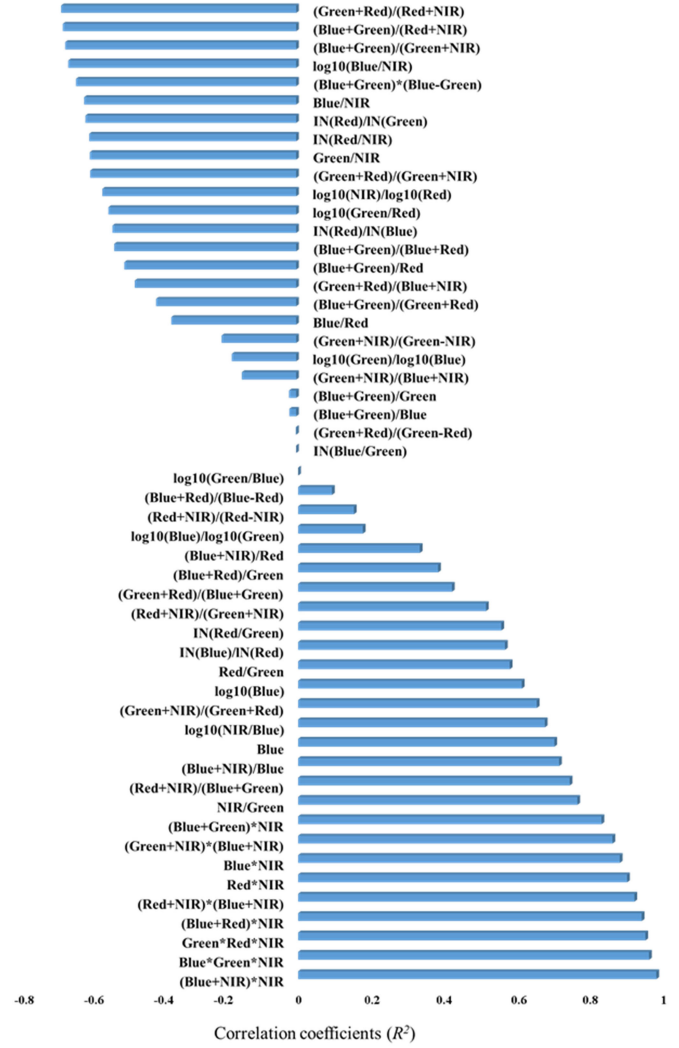


Fig. 2. Correlation coefficients ( $R^2$ ) between various band combinations from Landsat images and Turbidity concentrations.

turbidity [see Fig. 3(a)–(i)]. The results indicate that all the established linear models are statistically significant ( $p$ -level  $< 0.001$ ). The regression models with high determination coefficient ( $R^2$ ) and high regression coefficient ( $R \sim 0.9$ ) were the models established by the three band combinations, i.e., (Blue+NIR)\*NIR, Blue\*Green\*NIR and Green\*Red\*NIR [see Fig. 3(a)–(c)]. To further verify the applicability and reliability of these models, the remaining 60 sample points were used for the subsequent model validation. The model validation results [see Fig. 4(a) and (b)] suggest that the RMSE values of Red\*NIR, (Blue+NIR)\*NIR, and (Green+NIR)\*(Blue+NIR) were quite low (23.72–25.81 NTU). In summary, the model with the highest correlation coefficient  $R^2$  and lowest RMSE value is the regression model with the independent variable (Blue+NIR)\*NIR [see Figs. 3(a) and 4(a)]. Finally, the regression model  $y = 8194.1x - 38.717$  (where  $x$  was the (Blue+NIR)\*NIR band combination value and  $y$  was the turbidity value) was selected as the turbidity evaluation model in the article.

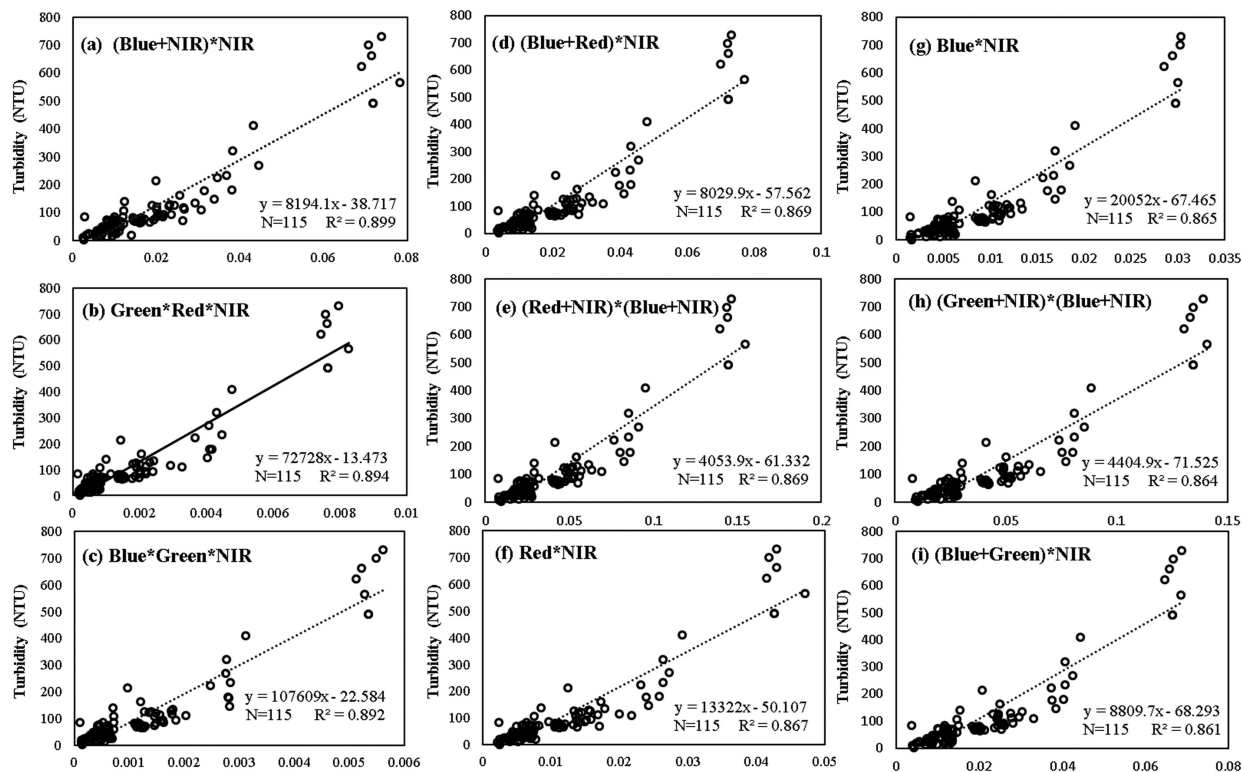


Fig. 3. Calibration and validation results of turbidity retrieval models based on 218 *in situ* samples. Note: (a)–(i) represent the dependence between the optimal band combinations with measured turbidity, respectively.

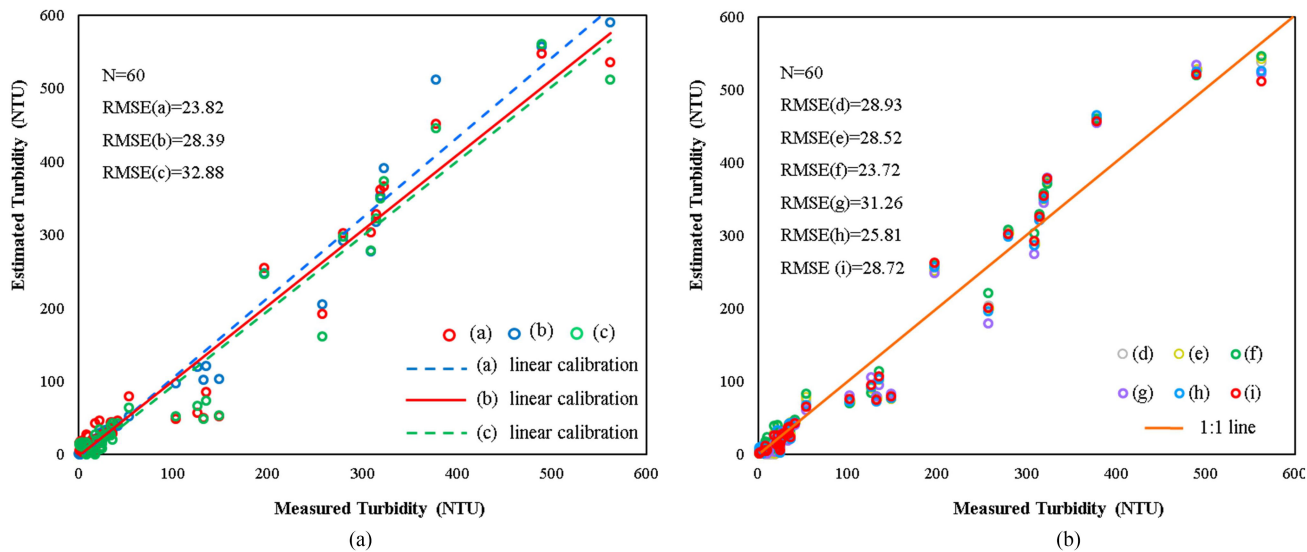


Fig. 4. (a)–(b) scatter plots showing comparison between the measured and estimated turbidity in water of testing samples (where the estimated turbidity is the turbidity value calculated by the simulation model established with the optimal band combination (a)–(i) in Fig. 3 as independent variables). All the correlations are statistically significant at the  $p$ -level  $< 0.001$ .  $N$  is the sum of samples in water (for interpretation of the references to color in this figure legend, the reader is referred to the Web version of this article).

### B. Turbidity Spatial Patterns of Turbidity

Figs. 5 and 7 present the spatial patterns of annual turbidity in the study area from 1984 to 2018. The results show that water turbidity of the Daqing lakes exhibited obvious spatial differences, with little change in trend over time. From the multiyear mean values of water turbidity of 15 typical lakes, we

can see that XDH had the highest turbidity value (448.1 NTU), followed by KL, DDH, and NYSK (turbidity ranged 215–265 NTU), then followed by YL, ZJT and HQRS (turbidity ranged 150–200 NTU) (see Fig. 7). These lakes with higher turbidity values are mostly distributed in the southern part of the study area or near the east-west central axis. Within the scope of the study

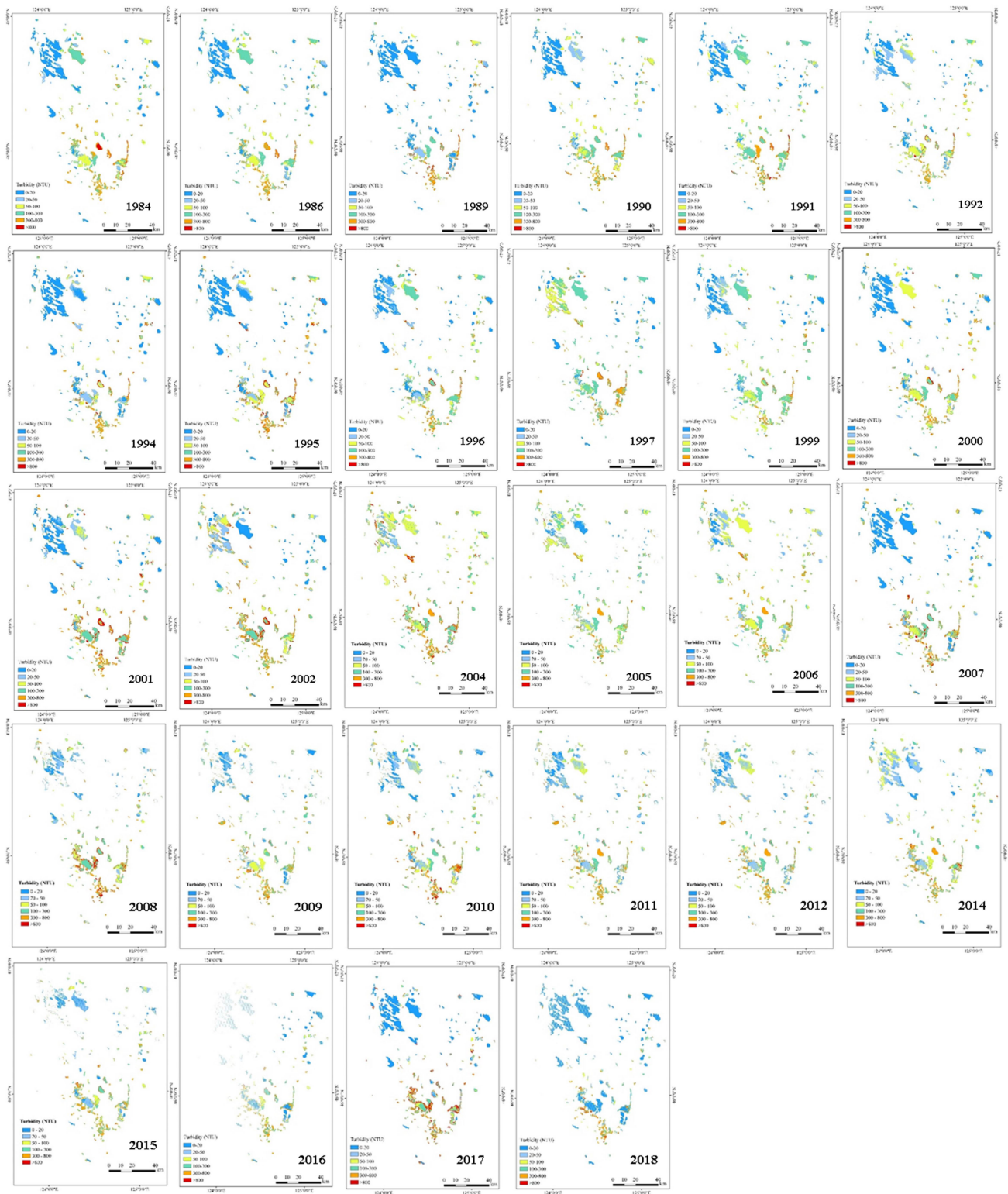


Fig. 5. Time series turbidity (1984–2018) estimated for the Daqing lakes.

area, lakes such as TLH, LH, and HSH had the lowest turbidity values (ranged 52.07–95.87 NTU) (see Fig. 7). These lakes with lower turbidity values are mostly large lakes distributed in the northeast of the study area (see Fig. 7). In general, the water turbidity of lakes in the study area demonstrated obvious

spatial distribution characteristics. More generally, the lakes in the south had higher turbidity; the lakes in the northwest had lower turbidity; the lakes in the east had turbidity lower than those in the south, and higher than those in the northwest (see Fig. 5).

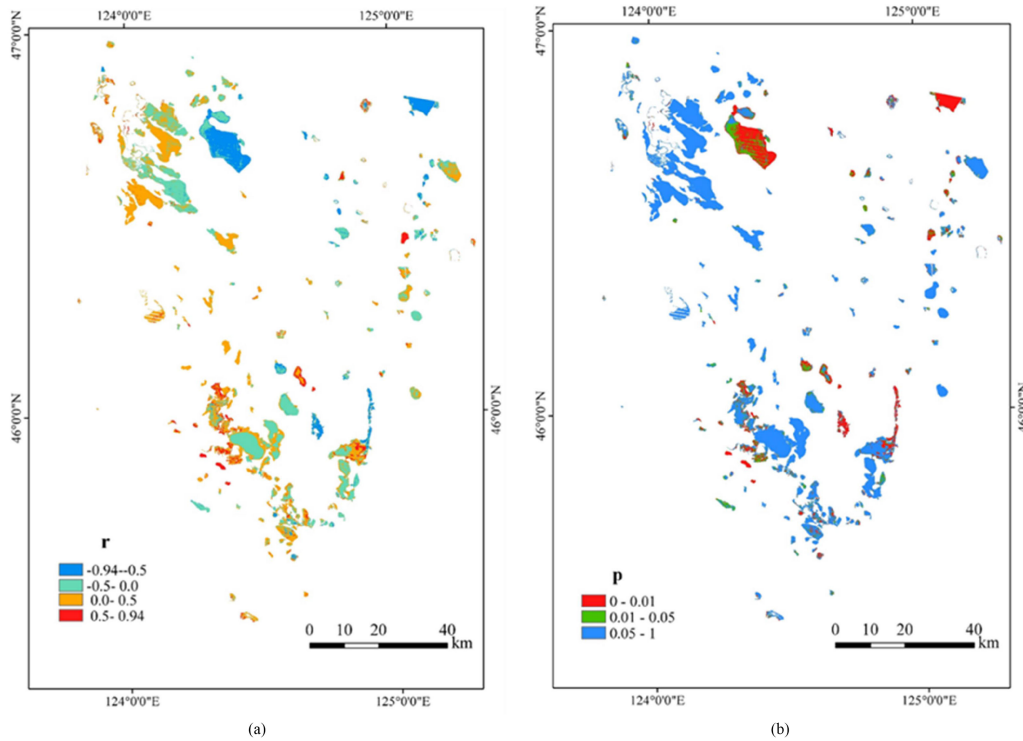


Fig. 6. Trend of Landsat-derived turbidity from 1984 to 2018. (a) Correlation between turbidity and years. (b) Reliability of the relationships.

### C. Turbidity Temporal Changes

Figs. 5 and 6 show the temporal variation of water turbidity in the Daqing Lakes from 1984 to 2018. The results indicate that the water turbidity of most of the Daqing lakes trended downward over the past 35 years, especially in the northwest and south of the study area (see Figs. 5 and 6). However, the water turbidity of several lakes in the southwest of the study area trended upward significantly (e.g., some small lakes around NYSK). In general, the water turbidity of the lakes fluctuated significantly over the past 35 years. It can be divided into three main periods: a significant downward trend in 1984–1995; a significant upward trend in 1996–2006; and another significant downward trend in 2007–2018 (see Fig. 5). From 1984 to 1995, the average turbidity value decreased from 171.7 to 119.2 NTU, with a decrease rate of 4.8 NTU per year. However, from 1996 to 2006, the average annual turbidity value increased from 159 to 240.1 NTU, with an increase rate of 8.1 NTU per year. From 2007 to 2018, the annual average turbidity value dropped from 188.62 to 123.14 NTU, with a decline rate of 5.95 NTU per year (see Fig. 6). In this article, the decreasing trend of turbidity was significantly greater than the increasing trend of turbidity, and the significance level of turbidity variation trend of more than 40% water was less than 0.05 [see Fig. 6(b)].

Fig. 7(a) illustrates the annual average turbidity changes of 15 typical lakes from 1984 to 2018. The results demonstrate that the average annual turbidity of most lakes trended downward from 1984 to 2018, with the most obvious trends in some large lakes (e.g., LH with a change rate of 5.04 NTU per year) and southern natural precipitation lakes (e.g., XDH with a change rate of 24.9 NTU per year). For some urban lakes, such as YL,

ZJT, and ZNP, the water turbidity values trended upward over time with 3.81, 3.65, and 3.72 NTU per year, respectively, (see Fig. 7).

Figs. 7(b) and 8 show the monthly average turbidity from April to October. In this article, turbidity showed obvious seasonal and monthly variations. The turbidity was the highest in May and the lowest in July; and increased again from late August to October. This result reflects the seasonal characteristics of water turbidity in lakes (spring > autumn > summer). Such regular seasonal and monthly changes can be observed in most water bodies. Nevertheless, the turbidity of several lakes still experienced significant difference from other lakes in monthly changes. For example, the turbidity of YL lake exhibited a significant upward trend in July.

## IV. DISCUSSION

### A. Model Assessment

Good correlations between remote sensing reflectivity and water quality parameters have been confirmed across a wide range of oceanic and inland waters by different research groups [64]–[66]. However, the inversion models applicable to different water quality parameters can vary due to regional and band sensitivity differences [67]–[69]. Landsat blue-green band and near-infrared band have strong water penetration ability and the ability to distinguish water clarity [70], [71]. Thus, their band combinations may be more sensitive to water turbidity parameters, which has also been further verified in this article [72], [73]. Therefore, we selected the most closely related nine combinations from hundreds of waveband combination calculation results to establish linear fitting with water turbidity. Among

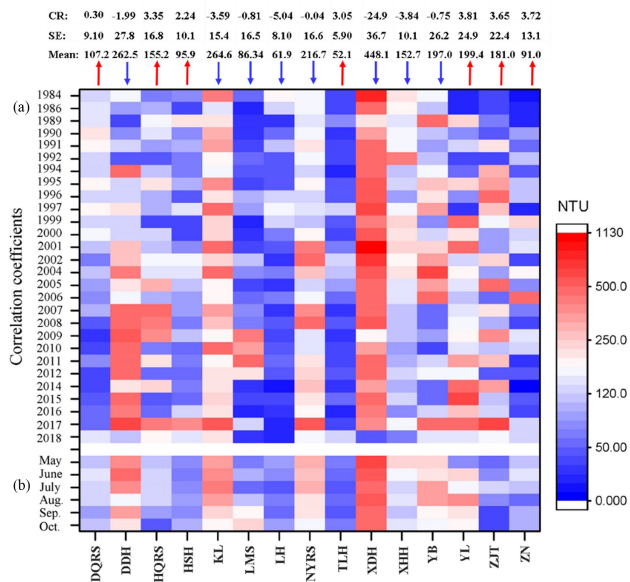


Fig. 7. (a) Annual series of turbidity from 1984 to 2018. (b) Monthly mean turbidity. Note: where each column represents a typical lake or reservoir, and each cell represents an annual mean turbidity value. \*\*CR and SE respectively represents change rate of turbidity and standard error from 1984 to 2018. The red and green arrows indicate that the turbidity of experienced a significant increasing or decreasing trend over 35 years, respectively (for interpretation of the references to color in this figure legend, the reader is referred to the Web version of this article).

these established remote sensing models, the (Blue+NIR)\*NIR linear model has demonstrated the greatest relative advantages (in terms of degree of correlation or small error coefficient), and it was considered the best choice. This is probably because this model is applicable to lakes with low and high turbidity, which can be widely implemented in this study or other areas with high turbidity (see Fig. 3). In this study area, lakes are dense and turbidity values spanned widely. Hence, after comprehensive comparison, the (Blue+NIR)\*NIR linear model is the most suitable. This article also found that the (Green + NIR) \*(Blue + NIR) linear fitting model might be the most suitable reference model for lakes with low turbidity values (e.g., < 200 NTU), which needs to be further validated in future studies. In addition, compared with the inversion results of water quality parameters from other studies, our turbidity assessment showed better model fitting degree and verification results [11], [52]. This might be partly because of the selection of the most suitable atmospheric correction method for class II water bodies, and partly because of the large data sampling points and volume used in this article. Our research results once again confirmed the superiority of Landsat remote sensing images in retrieving and analyzing the long-term water quality parameters.

### B. Spatiotemporal Pattern of Turbidity

Overall, the water turbidity of the lakes was high in the south, low in the northwest and moderate in the east. This spatial pattern might be affected by natural factors (e.g., lake area and location) and human interference (e.g., land use). XDH, KL, DDH, and NYSK with highest turbidity values (above 200 NTU) are all

located in the southern part of the Daqing Lakes [see Figs. 7(a) and 5]. This area is Daqing's main industrial district, and there are two large chemical plants and power plants around the lakes. Moreover, XDH has the smallest area and shallowest water depth, and it is also a typical precipitation lake. Therefore, the water turbidity of XDH was the highest, followed by KL, DDH, and NYSK. At the same time, the turbidity values of YL, ZJT, HQRS, and other lakes located in the east of the Daqing Lakes were also higher than those in the west. This is because these lakes are located in the main urban area of Daqing city, which has the largest population and domestic sewage discharge in Daqing city. In particular, YL is not only a typical urban lake, but also an important oil mining lake. In the whole study area, the lakes with the lowest water turbidity were all clustered in the western part of the Daqing Lakes. This may be because the lakes in this region are densely distributed, and most of them have large water volume, deep water and large area, but are less affected by human disturbance.

The annual turbidity from 1984 to 2018 (see Fig. 5) and monthly turbidity from May to October (see Fig. 8) were mapped for the Daqing Lakes. Due to the influence of clouds, some images of missing years or turbidity of water (colorless dots in Fig. 5) were not shown in this article. Nevertheless, the absence of turbidity information in a few pixels or a few years does not affect the overall trend [74]–[76]. In the past 35 years, two significant fluctuations of water turbidity occurred mainly in 1996–2006 (uptrend) and 2007–2018 (downtrend) (see Fig. 5). The first obvious upswing of water turbidity in Daqing Lakes occurred after 1995 because of rapid population growth; the fastest urban construction speed; the greatest agricultural fertilizer application; and the largest discharge of industrial water and domestic sewage in this area. However, the second significant downswing of turbidity in Daqing Lakes was after 2006. This is mainly because China and Daqing municipal government issued a series of water environment treatment measures from 2006 to 2010. Daqing municipal government has performed comprehensive treatment of industrial wastewater and domestic sewage; reduced the amount of fertilizer used in farmland; and improved residents' awareness of environmental protection. These led to the gradual and continuous decrease of water turbidity [45]. The time series analysis results of water turbidity in this article have verified our previous hypothesis to a certain extent, which are similar to the TSM time variation trend of Du *et al.*, but not exactly the same [11]. Du *et al.* found that TSM in a large area of water bodies in the Songnen Plain showed a decreasing trend year by year, while our study found that the turbidity of water bodies in Daqing lakes showed an overall decreasing trend, but there were two obvious rising stages due to the influence of human disturbance, such as urban construction and policies. On the one hand, the two study areas overlap but are not exactly the same; on the other hand, although turbidity and TSM index are correlated to a certain extent, the influencing factors of water turbidity are very complex. TSM is not the only factor affecting water turbidity, so it cannot be completely judged by TSM state.

The monthly mean turbidity of most lakes varied significantly with some periodic characteristics (see Fig. 8). The water turbidity value in April and May was the highest, and it dropped



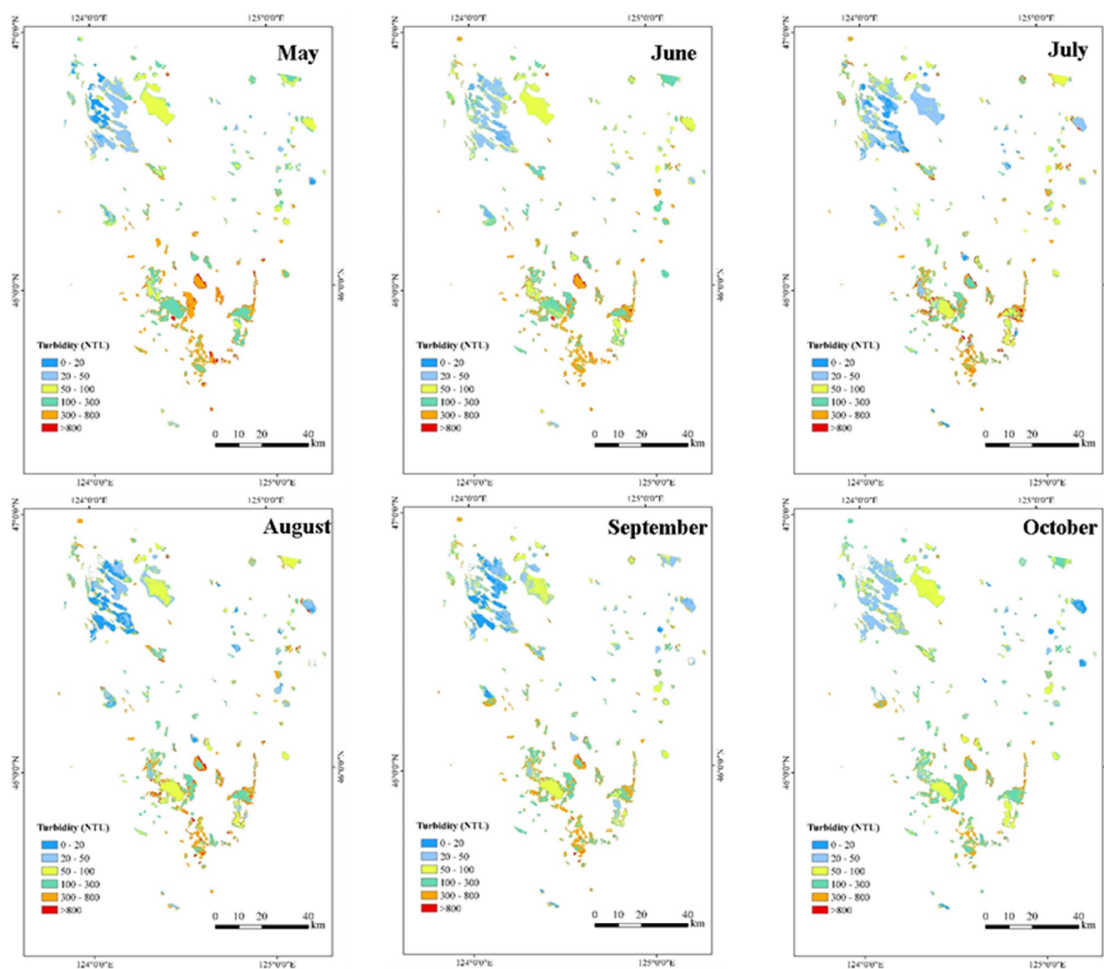


Fig. 8. Maps of monthly mean turbidity (NTU) derived from Landsat images. Note: The values were computed as the monthly mean using the entire times series of observations (1984–2018).

to the lowest in July and August, and then increased again in September and October. These typical monthly changes might be closely related to the unique climatic factors in Northeast China. Basically, April and May are part of spring in Northeast China. During this period, the ice and snow on the lake surface melts, the wind speed increases, and the sediment in the lake suspension occurs frequently, so the water turbidity of the lake could increase significantly. However, in July and August, which is the summer in Northeast China, the wind speed weakens, the snow and ice melt down, and the lake sediment disturbance is relatively small, so the water turbidity in this period could be the lowest throughout the year. In late September, the wind speed increases again, the frequency of sediment disturbance increases continuously, and the turbidity could increase. In October, due to the unique climate in Northeast China, the lake surface begins to freeze again, and turbidity could stay at a high level. After November, the ice builds up and the turbidity could drop. However, this article could not obtain the remote sensing image of the real water body of the lake after freezing. In general, the monthly and seasonal changes of water turbidity in lakes might be driven by the influence of wind, temperature and other natural factors. Moreover, these satellite image-based predictions are quite consistent with our field investigations.

### C. Driving Factors for Turbidity Variation

To further understand the spatiotemporal variation mechanism of water turbidity in lakes of this region, we further discuss the influencing factors of water turbidity in this section. In addition to some human factors, many studies also suggested that water turbidity may be related to some natural factors, such as wind speed and precipitation [77]–[79]. First of all, we analyzed the data of lake area, water temperature and water depth to understand the relationship between these factors and turbidity of water. Numerically, the lake water depth, water temperature and area can be divided into five to six categories. Interestingly, turbidity value showed a very obvious gradient change trend with these factors. Fig. 9(a)–(c) reveals that as the depth deepens, the water temperature decreases and the area increases, thus the water turbidity of the lake drops down. On the contrary, the water turbidity of lake gradually increases with the shallow water depth, rising water temperature, and shrinking area of the lake. This result once again proved the close relationship between water turbidity and the lake ambient environment. Generally speaking, a smaller lake is primarily formed by precipitation, and its area size varies with the amount of precipitation at that time [80]. At the same time, a small lake generally has shallow water

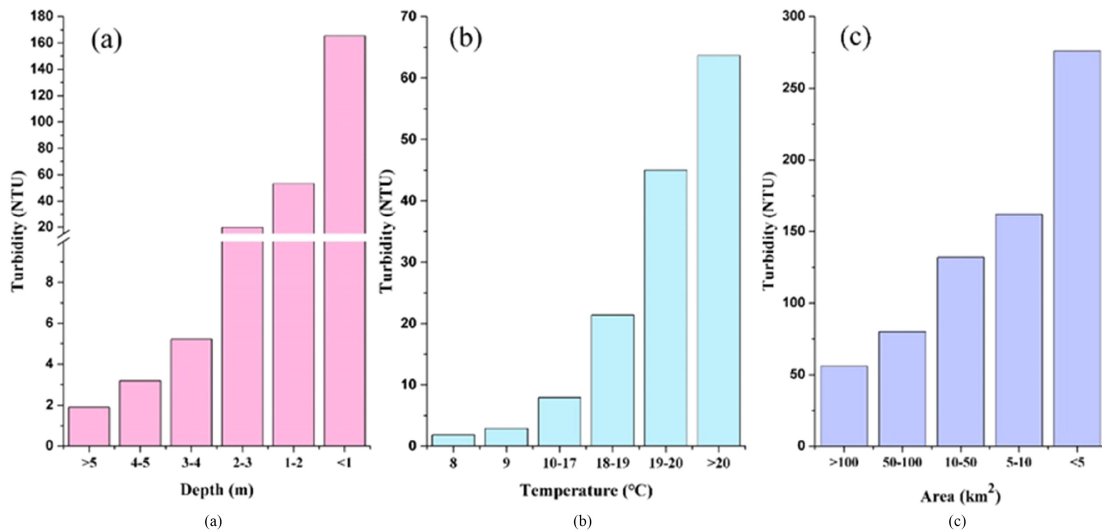


Fig. 9. Comparison between lake/reservoir depth, water temperature, area, and turbidity.

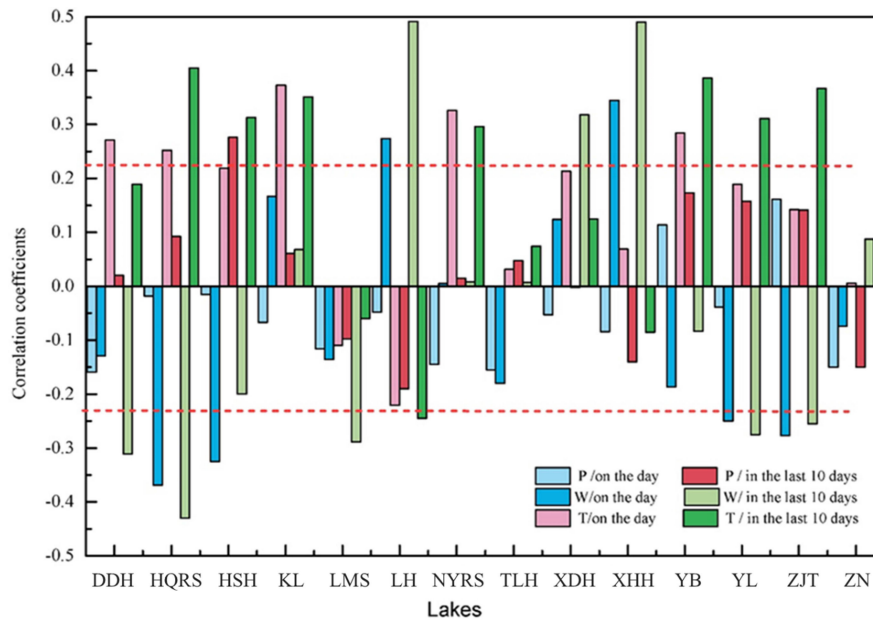


Fig. 10. Correlation coefficients ( $R$ ) between annual mean turbidity and meteorological factors, where  $P$  is precipitation/cumulative precipitation,  $W$  is wind speed and  $T$  is Temperature. Note: The red dashed lines indicate the critical values for which the relationships are statistically significant if the coefficient is above the positive value or below the negative value ( $p < 0.05$ ) (for interpretation of the references to color in this figure legend, the reader is referred to the web version of this article).

depth and relatively high water temperature characteristics. A small and shallow lake is easily disturbed by sediment, and the sediment on its shore is easily carried into the lake by wind [11]. These processes contribute greatly to the increase of water turbidity of a lake. However, a low-temperature and deep-water lake with large area is less disturbed by sediment, and the amount of wind-sand carried into the lake is relatively small, so its water turbidity is relatively low.

Wind, temperature and precipitation factors are important meteorological factors, which regulate the turbidity of inland or coastal waters and affect the movement of lake sediments [81]–[85]. To further explore the relationship between climatic

factors and water turbidity and understand the potential meteorological factors of interannual turbidity variation, we analyzed the correlation between the average turbidity of each lake in each landscape image and local wind, temperature, and precipitation (which were collected from the National Meteorological Information Center.<sup>2</sup> These climate data mainly include the averaged wind speed, averaged temperature and cumulative precipitation data (e.g., of the day, the last ten days when the satellite image was captured) from corresponding five meteorological stations (see Fig. 10).

<sup>2</sup>[Online]. Available: <http://data.cma.cn/>

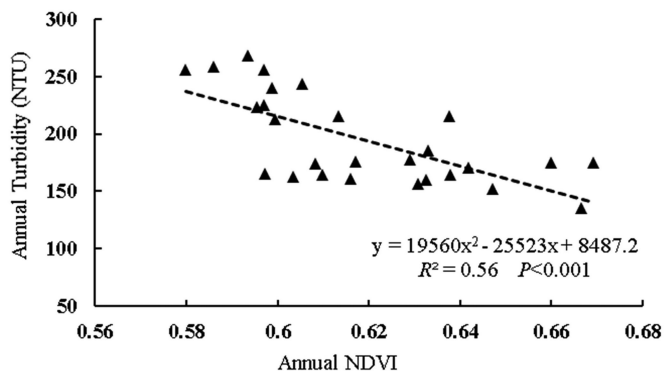


Fig. 11. Relationship between annual mean NDVI and annual mean Turbidity in the study area.

The average water turbidity of most lakes demonstrate positive correlations with temperature and wind speed ( $R < 0.5$ ). Since temperature change is not obvious in the short term, the correlation between temperature and water turbidity on the day of image acquisition and in the past ten days is similar. By contrast, the correlations between water turbidity and precipitation are mostly statistically insignificant, especially the daily precipitation ( $p > 0.05$ ). However, in several small shallow-water lakes that rely on precipitation, the correlation between turbidity and cumulative precipitation over the past ten days is weak. This is probably because the study area is dominated by semiarid climate with little rainfall and high wind all year round. Therefore, temperature and wind seem to have a greater effect on turbidity than rainfall, especially the temperature factor. For a few lakes, the water turbidity is not consistent with temperature and wind speed, which may be affected by other human activities, such as land use.

To further investigate the influencing factors of water turbidity in lakes, we also analyze human activities, such as land use around the lake. Some lakes are located around farmland or saline-alkali land. When the land around the lakes is affected by soil erosion, sediment will be transported into the lakes [11], [52]. In this circumstance, vegetation cover is an important factor that affects the degree of soil erosion and the ecological environment of lakes. Therefore, the NDVI index of vegetation coverage in the study area from 1984 to 2018 is calculated to explore the relationship between vegetation coverage and water turbidity. The linear regression model shows that the annual average turbidity is highly correlated with the annual average NDVI ( $p < 0.001$ ), and presents a better linear fitting relationship (see Fig. 11). Preliminarily, we deduce that the vegetation coverage around the lake is also one of the key factors affecting the water turbidity. This also proves once again that turbidity, an important index representing the state of water environment in lakes, is subjected to the comprehensive action of various natural factors and human activities. Due to data scarcity, only several possible factors that affect water turbidity are explored here. In the future, it would be interesting to explore the relationship between water turbidity and other potential factors (e.g., biogeochemistry and morphology) to improve water resource management.

## V. CONCLUSION

Based on extensive field measurements and Landsat image data, this article developed an empirical model for estimating water turbidity; and mapped the spatiotemporal patterns of water turbidity of the Daqing Lakes in Northeast China in order to explore the reasons of the spatial and temporal differences of water turbidity. First, we demonstrated the potential of using historical Landsat TM imagery combined with field survey data to map the spatiotemporal patterns of turbidity in inland waters. Through the comparison of multiband combined operation results, we confirmed that the linear model (Blue+NIR)\*NIR is more suitable for the assessment of water turbidity in Daqing lakes. Second, in terms of spatial pattern, the water turbidity values of Daqing Lakes present obvious distribution pattern of high in the south; low in the northwest; and moderate in the east. This spatial pattern might be caused by the joint action of natural factors (e.g., lake area and location) and human factors (e.g., surrounding land use). Third, in terms of temporal trend, the turbidity of most lakes decreased with time in the past 35 years. However, from 1996 to 2006, due to urban development, production and domestic sewage discharge and lack of timely treatment, turbidity fluctuated significantly. Turbidity of all water bodies generally decreased from May to the lowest level in July and then increased from September onward, which may be closely related to the unique climatic factors in Northeast China. Finally, we further analyzed the relationship between some typical elements and turbidity to confirm the influencing factors of water turbidity. Our study revealed the close relationship between turbidity and lake area, water temperature and water depth, as well as the potential role of temperature and regional vegetation coverage in regulating turbidity change. In addition, the implementation of national and local water environmental protection policies contributed significantly to the reduction of water turbidity, indicating the effectiveness of water resource management practices. The results provide important information for the water quality management and protection in China and highlight the significance of satellite remote sensing in large-scale and long-term monitoring of water quality in lakes.

## ACKNOWLEDGMENT

Data were provided by the USGS through Google Earth Engine cloud computation platform. The authors would like to thank Y. Zhao, T. Shao, J. Ma, J. Xu, and M. Wang for assistance with data collection and processing. The authors would like to express their gratitude to EditSprings<sup>3</sup> for the expert linguistic services provided.

## REFERENCES

- [1] Q. Guan, L. Feng, X. Hou, G. Schurgers, and J. Tang, "Eutrophication changes in fifty large lakes on the Yangtze Plain of China derived from MERIS and OLCI observations," *Remote Sens. Environ.*, vol. 246, 2020, Art. no. 111890.
- [2] N. A. Bakunov, D. Y. Bol'Shiyanov, S. A. Pravkin, and A. S. Makarov, "Sorption-diffusion model of 137 CS absorption by bottom deposits of lakes in the reconstruction of 137 CS fallout to water basins," *Radiochemistry*, vol. 62, pp. 667–672, 2020.

<sup>3</sup>[Online]. Available: <https://www.editsprings.com/>

- [3] D. M. Bezmaternykh and O. N. Vdovina, "Trophic structure of benthic macroinvertebrate communities from lakes with various water-salinity levels," *Inland Water Biol.*, vol. 13, pp. 62–68, 2020.
- [4] M. Opat, R. Augustyniak, J. Grochowska, K. Parszuto, and G. Winiewski, "Behavior of aluminum compounds in soft-water lakes subjected to experimental reclamation with polyaluminum chloride," *Water Air Soil Pollut.*, vol. 231, no. 358, pp. 1–11, 2020.
- [5] C. A. Varotsos, V. F. Krapivin, F. A. Mkrtchyan, S. A. Gevorkyan, and T. Cui, "A novel approach to monitoring the quality of lakes water by optical and modeling tools: Lake Sevan as a case study," *Water Air Soil Pollut.*, vol. 231, no. 435, pp. 1–15, 2020.
- [6] T. Sun, W. Q. Cheng, Q. Y. Bo, X. Meng, and D. Liang, "Analysis on historical flood and countermeasures in prevention and control of flood in Daqing River Basin," *Environ. Res.*, vol. 196, 2021, Art. no. 11089511.
- [7] W. Mu, F. Yu, Y. Han, W. Ma, and Y. Zhao, "Meteorological drought risk in the Daqing River Basin, North China: Current observations and future projections," *Stochastic Environ. Res. Risk Assessment*, vol. 34, pp. 1795–1811, 2020.
- [8] M. Shen *et al.*, "Sentinel-3OLCI observations of water clarity in large lakes in Eastern China: Implications for SDG 6.3.2 evaluation," *Remote Sens. Environ.*, vol. 247, 2020, Art. no. 111950.
- [9] P. M. Vitousek, S. Hättenschwiler, L. Olander, and S. Allison, "Nitrogen nature," *Ambio*, vol. 31, pp. 97–101, 2002.
- [10] W. Liu, Q. Zhang, and G. Liu, "Lake eutrophication associated with geographic location, lake morphology and climate in China," *Hydrobiologia*, vol. 644, pp. 289–299, 2010.
- [11] Y. X. Du *et al.*, "Quantifying total suspended matter (TSM) in waters using landsat images during 1984–2018 across the Songnen Plain, Northeast China," *J. Environ. Manage.*, vol. 262, 2020, Art. no. 110334.
- [12] S. Chang *et al.*, "Pollution distribution characteristics and risk assessment of polycyclic-aromatic hydrocarbons in surface water and sediment of Beijiang river," *J. Northwest Univ.*, vol. 1, pp. 56–67, 2020.
- [13] S. Hilt, I. Henschke, J. Rücker, and B. Nixdorf, "Can submerged macrophytes influence turbidity and Trophic state in deep lakes? Suggestions from a case study," *J. Environ. Qual.*, vol. 39, pp. 725–733, 2010.
- [14] R. M. Almeida, F. Roland, S. J. Cardoso, V. F. Farjalla, R. L. Bozelli, and N. O. Barros, "Viruses and bacteria in floodplain lakes along a major Amazon tributary respond to distance to the Amazon river," *Front. Microbiol.*, vol. 6, 2020.
- [15] A. Negoitescu, A. Tokar, C. Hamat, "The influence of the air thermal and rainfall regimes on storage lakes water turbidity," *Materiale Plastice*, vol. 53, no. 3, pp. 542–545, 2016.
- [16] M. N. Castillo, J. P. Lowry, and J. S. R. Paling, "Testing the waters: Tzeltal maya rituals, reconnaissance, and survey of lakes in the Lacanhá Basin, Chiapas, Mexico," *J. Maritime Archaeol.*, vol. 15, pp. 451–474, 2020.
- [17] X. Zhang, X. Mei, and R. D. Gulati, "Effects of omnivorous tilapia on water turbidity and primary production dynamics in Shallow lakes: Implications for ecosystem management," *Rev. Fish Biol. Fisheries*, vol. 27, pp. 245–254, 2017.
- [18] L. Sun, X. Z. Liang, T. Ling, M. Xu, and X. Lee, "Improving a multilevel turbulence closure model for a Shallow lake in comparison with other 1-D models," *J. Adv. Model. Earth Syst.*, vol. 12, pp. 1–23, 2020.
- [19] K. Dörnhöfer and N. Oppelt, "Remote sensing for lake research and monitoring – recent advances," *Ecol. Indicators*, vol. 64, pp. 105–122, 2016.
- [20] F. C. J. M. Roozen, G. J. V. Geest, B. W. Ibelings, R. Roijackers, M. Scheffer, and A. D. Buijse, "Lake age and water level affect the turbidity of floodplain lakes along the lower Rhine," *Freshwater Biol.*, vol. 48, pp. 519–531, 2010.
- [21] J. P. M. Vink, R. N. J. Comans, J. J. Dijkstra, and L. P. M. Lamers, "Soils in lakes: The impact of inundation and storage on surface water quality," *Environ. Monit. Assessment*, vol. 192, pp. 1–18, 2020.
- [22] K. S. Song *et al.*, "Water quality monitoring using landsat thematic mapper data with empirical algorithms in Chagan Lake, China," *J. Appl. Remote Sens.*, vol. 5, pp. 1–21, 2011.
- [23] S. Y. Son and M. H. Wang, "VIIRS-derived water turbidity in the great lakes," *Remote Sens.*, vol. 11, no. 12, pp. 1112–1448, 2019.
- [24] L. Wei, Y. Liu, C. M. Mannaerts, G. Wu, "Monitoring variation of water turbidity and related environmental factors in Poyang Lake National Nature Reserve, China," *Proc. SPIE.*, vol. 6754, 2007, Art. no. 67541H.
- [25] A. T. Vafeidis *et al.*, "A new global coastal database for impact and vulnerability analysis to sea-level rise," *J. Coastal Res.*, vol. 24, pp. 917–924, 2008.
- [26] S. Tao *et al.*, "Changes in China's lakes: Climate and human impacts," *Nat. Sci. Rev.*, vol. 7, pp. 132–140, 2019.
- [27] S. Wang, J. Li, B. Zhang, Z. Lee, and X. Zhang, "Changes of water clarity in large lakes and reservoirs across China observed from long-term MODIS," *Remote Sens. Environ.*, vol. 247, 2020, Art. no. 111949.
- [28] J. Lu, Z. Liu, W. Liu, X. Chen, and L. Zhang, "Assessment of CFSR and CMADS weather data for capturing extreme hydrologic events in the Fuhe River Basin of the Poyang Lake," *Jawra J. Amer. Water Resour. Assoc.*, vol. 56, pp. 917–934, 2020.
- [29] F. Lian, C. M. Hu, X. L. Chen, X. B. Cai, L. Q. Tian, and W. X. Gan, "Assessment of inundation changes of Poyang Lake using MODIS observations between 2000 and 2010," *Remote Sens. Environ.*, vol. 121, pp. 80–92, 2012.
- [30] C. Giardino, V. E. Brando, A. G. Dekker, N. Strombeck, and G. Candiani, "Assessment of water quality in lake Garda (Italy) using hyperion," *Remote Sens. Environ.*, vol. 109, pp. 183–195, 2007.
- [31] H. Duan, R. Ma, Y. Zhang, and Z. Bai, "Remote-sensing assessment of regional inland lake water clarity in Northeast China," *Limnology*, vol. 10, 2009, Art. no. 135.
- [32] J. Wang and Z. Zhang, "Phytoplankton, dissolved oxygen and nutrient patterns along a Eutrophic river-estuary continuum: Observation and modeling," *J. Environ. Manage.*, vol. 261, 2020, Art. no. 110233.
- [33] C. Guo, Y. Chen, R. E. Gozlan, H. Liu, and L. Wang, "Patterns of fish communities and water quality in impounded lakes of China's South-to-North water diversion project," *Sci. Total Environ.*, vol. 713, 2020, Art. no. 136515.
- [34] J. Ndungu, B. C. Monger, D. C. M. Augustijn, S. J. M. H. Hulscher, N. Kitaka, and J. M. Mathooko, "Evaluation of spatio-temporal variations in chlorophyll-a in Lake Naivasha, Kenya: Remote-sensing approach," *Int. J. Remote Sens.*, vol. 34, no. 21/22, 2013, Art. no. 8142–8155.
- [35] D. Passang, F. Peter, and B. A. Mark, "A semi-analytic model for estimating total suspended sediment concentration in turbid coastal waters of Northern Western Australia using MODIS-aqua 250 m data," *Remote Sens.*, vol. 8, no. 7, pp. 1–23, 2016.
- [36] G. Bitelli and E. Mandanici, "Atmospheric correction issues for water quality assessment from remote sensing: The case of Lake Qarun (Egypt)," in *Proc. Earth Resour. Environ. Remote Sens./GIS Appl.*, vol. 7831, 2010, pp. 1–8.
- [37] T. Asmare, B. Demissie, A. G. Nigusse, and A. Gebrekidan, "Detecting spatiotemporal expansion of water hyacinth (*Eichhornia crassipes*) in Lake Tana, Northern Ethiopia," *J. Indian Soc. Remote Sens.*, vol. 48, pp. 751–764, 2020.
- [38] D. Doxaran, R. C. N. Cherukuru, and S. J. Lavender, "Inherent and apparent optical properties of turbid estuarine waters: Measurements, modelling and application to remote sensing," *Appl. Opt.*, vol. 45, pp. 2310–2324, 2006.
- [39] K. R. Christianson, B. M. Johnson, and M. B. Hooten, "Compound effects of water clarity, inflow, wind and climate warming on mountain lake thermal regimes," *Aquatic Ecos.*, vol. 82, pp. 6.1–6.17, 2020.
- [40] S. C. Yao, B. Xue, X. G. Lu, and H. F. Xiao, "The hydrochemical characteristic of lakes in Songnen Plain," *Wetland Sci.*, vol. 8, no. 2, pp. 169–175, 2010.
- [41] A. G. Dekker, R. J. Vos, and S. W. Peters, "Comparison of remote sensing data, model results and in situ data for total suspended matter (TSM) in the southern Frisian Lakes," *Sci. Total Environ.*, vol. 268, pp. 197–214, 2001.
- [42] L. Luo, D. Mao, Z. Wang, B. Zhang, C. Ren, and M. Jia, "Analysis of dynamics and driving forces of lakes and reservoirs in Western Songnen Plain," *Ransactions Chin. Soc. Agricultural Eng.*, vol. 31, no. 22, pp. 285–291, 2015.
- [43] F. Sui, S. Zang, Y. Fan, and H. Ye, "Effects of different saline-alkaline conditions on the characteristics of phytoplankton communities in the lakes of Songnen Plain," *China Plos One*, vol. 11, no. 10, 2016, Art. no. 0164734.
- [44] Q. Chen, K. Tan, C. Zhu, and L. I. Ruonan, "Development and application of a two-dimensional water quality model for the Daqinghe River mouth of the Dianchi Lake," *J. Environ. Sci.*, vol. 21, pp. 313–318, 2009.
- [45] X. D. Wang and S. Y. Zang, "Distribution characteristics and ecological risk assessment of toxic heavy metals and metalloids in surface water of lakes in Daqing Heilongjiang Province, China," *Ecotoxicology*, vol. 23, pp. 609–617, 2014.
- [46] X. D. Wang, S. Y. Zang, and X. D. Na, "Analyzing dynamic process of land use change in Ha-DaQi industrial corridor of China," *Procedia Environ. Sci.*, vol. 11, pp. 1008–1015, 2011.
- [47] Q. I. Fu-Li, L. I. Yong-Li, F. L. Zhang, L. U. Shou-Gang, and Y. C. Bai, "Evaluation of geothermal resources in Heiyu lake area in Daqing city of Heilongjiang province," *Hydrogeol. Eng. Geol.*, vol. 39, pp. 139–142, 2012.

- [48] S. F. Zheng, B. Zhang, S. Y. Zang, Z. M. Wang, K. S. Song, and D. W. Liu, "Impact of industrial structure on LUCC in Daqing city of Heilongjiang province," *Resour. Sci.*, vol. 6, pp. 128–132, 2007.
- [49] N. Jing, Z. S. Wen, W. Lei, and K. W. Hui, "Spatial-temporal characteristics of land degeneration in resources-based cities: A case study in Daqing city in Heilongjiang province," *Resour. Sci.*, vol. 29, pp. 77–84, 2007.
- [50] S. Constantin, D. Doxaran, and T. Constantinescu, "Estimation of water turbidity and analysis of its spatio-temporal variability in the Danube River plume (Black Sea) using MODIS satellite data," *Continental Shelf Res.*, vol. 112, pp. 14–30, 2016.
- [51] S. M. Kloiber, P. L. Brezonik, L. G. Olmanson, and M. E. Bauer, "A procedure for regional lake water clarity assessment using landsat multispectral data," *Remote Sens. Environ.*, vol. 82, pp. 38–47, 2002.
- [52] K. S. Song *et al.*, "Quantification of lake clarity in China using landsat OLI imagery data," *Remote Sens. Environ.*, vol. 243, 2020, Art. no. 111800.
- [53] L. G. Olmanson, M. E. Bauer, and P. L. Brezonik, "A 20-year landsat water clarity census of Minnesota's 10,000 lakes," *Remote Sens. Environ.*, vol. 112, pp. 4086–4097, 2008.
- [54] I. M. McCullough, C. S. Loftin, and S. A. Sader, "Combining lake and watershed characteristics with landsat TM data for remote estimation of regional lake clarity," *Remote Sens. Environ.*, vol. 123, pp. 109–115, 2012.
- [55] B. Nechad, K. G. Ruddick, and G. Neukermans, "Calibration and validation of a generic multisensor algorithm for mapping of turbidity in coastal waters," *Proc. SPIE, Int. Soc. Opt. Eng.*, vol. 7473, 2009, Art. no. 74730H.
- [56] S. V. Balasubramanian, N. Pahlevan, B. Smith, C. Binding, and E. Boss, "Robust algorithm for estimating total suspended solids (TSS) in inland and nearshore coastal waters," *Remote Sens. Environ.*, vol. 246, 2020, Art. no. 111768.
- [57] R. L. Iles, D. W. Nan, J. R. White, and R. V. Rohli, "Impacts of a major Mississippi River freshwater diversion on suspended sediment plume kinematics in lake Pontchartrain, a semi-enclosed Gulf of Mexico estuary," *Estuaries Coasts*, vol. 44, 2020.
- [58] J. Ma, H. Duan, L. He, M. Tiffany, and X. Xu, "Spatiotemporal pattern of gypsum blooms in the Salton Sea, California, during 2000–2018," *Int. J. Appl. Earth Observ. Geoinf.*, vol. 89, 2020, Art. no. 102090.
- [59] C. M. Hu, "A novel ocean color index to detect floating algae in the global oceans," *Remote Sens. Environ.*, vol. 113, pp. 2118–2129, 2009.
- [60] X. W. Yang *et al.*, "Changes in area and water volume of the Aral Sea in the arid Central Asia over the period of 1960–2018 and their causes," *Catena Catena*, vol. 191, 2020, Art. no. 104566.
- [61] C. Kuhn and A. D. M. Valerio, "Performance of landsat-8 and sentinel-2 surface reflectance products for river remote sensing retrievals of chlorophyll-a and turbidity," *Int. J. Remote Sens. Environ.*, vol. 224, pp. 104–118, 2019.
- [62] R. S. Defries and J. R. G. Townshend, "NDVI-derived land cover classifications at a global scale," *Int. J. Remote Sens.*, vol. 15, no. 17, pp. 3567–3586, 1994.
- [63] G. L. Feyisa, H. Meilby, R. Fensholt, and S. R. Proud, "Automated water extraction index: A new technique for surface water mapping using landsat imagery," *Remote Sens. Environ.*, vol. 140, pp. 23–35, 2014.
- [64] S. Garaba, A. Friedrichs, D. Voß, and O. Zielinski, "Classifying natural waters with the Forel-Ule Colour index system: Results, applications, correlations and crowdsourcing," *Int. J. Environ. Res. Public Health*, vol. 12, no. 12, pp. 16096–16109, 2015.
- [65] J. Li *et al.*, "MODIS observations of water color of the largest 10 lakes in China between 2000 and 2012," *Int. J. Digit. Earth*, vol. 9, no. 8, pp. 788–805, 2016.
- [66] J. Pitarch, H. J. V. D. Woerd, R. J. W. Brewin, and O. Zielinski, "Optical properties of Forel-Ule water types deduced from 15 years of global satellite ocean color observations," *Remote Sens. Environ.*, vol. 231, 2019, Art. no. 111249.
- [67] Z. Duan and W. G. M. Bastiaanssen, "Estimating water volume variations in lakes and reservoirs from four operational satellite altimetry databases and satellite imagery data," *Remote Sens. Environ.*, vol. 134, pp. 403–416, 2013.
- [68] J. F. Crétaux *et al.*, "Absolute calibration or validation of the altimeters on the Sentinel-3A and the Jason-3 over lake Issykkul (Kyrgyzstan)," *Remote Sens.*, vol. 10, 2018, Art. no. 1679.
- [69] Y. Fang *et al.*, "Assessment of water storage change in China's lakes and reservoirs over the last three decades," *Remote Sens.*, vol. 11, 2019, Art. no. 1467.
- [70] M. J. Fernandes, C. Lázaro, A. L. Nunes, and R. Scharroo, "Atmospheric corrections for altimetry studies over inland water," *Remote Sens.*, vol. 6, pp. 4952–4997, 2014.
- [71] C. Hwang *et al.*, "Multi-decadal monitoring of lake level changes in the Qinghai-Tibet plateau by the climate implication," *Remote Sens.*, vol. 8, no. 6, pp. 1–21, 2016.
- [72] L. Ji and K. Gallo, "An agreement coefficient for image comparison," *Photogramm. Eng. Remote Sens.*, vol. 72, no. 7, pp. 823–833, 2006.
- [73] T. A. Keys and D. T. Scott, "Monitoring volumetric fluctuations in tropical lakes and reservoirs using satellite remote sensing," *Lake Reservoir Manag.*, vol. 34, no. 2, pp. 154–166, 2018.
- [74] C. M. Hu, Z. Q. Chen, T. D. Clayton, P. Swarzenski, J. C. Brock, and F. E. Muller-Karger, "Assessment of estuarine water-quality indicators using MODIS medium-resolution bands: Initial results from Tampa Bay, FL," *Remote Sens. Environ.*, vol. 93, pp. 423–441, 2004.
- [75] Z. Cao, H. Duan, L. Feng, R. Ma, and K. Xue, "Climate- and human-induced changes in suspended particulate matter over Lake Hongze on short and long timescales," *Remote Sens. Environ.*, vol. 192, pp. 98–113, 2017.
- [76] L. Feng, C. Hu, X. Chen, X. Cai, L. Tian, and W. Gan, "Assessment of inundation changes of Poyang Lake using MODIS observations between 2000 and 2010," *Remote Sens. Environ.*, vol. 121, pp. 80–92, 2012.
- [77] A. Arsen, J. F. Crétaux, M. Berge-Nguyen, and R. D. Rio, "Remote sensing-derived bathymetry of Lake Poopó," *Remote Sens.*, vol. 6, pp. 407–420, 2013.
- [78] S. Biancamaria, D. P. Lettenmaier, and T. M. Pavelsky, "The SWOT mission and its capabilities for land hydrology," *Remote Sens. Water Resour.*, vol. 5, pp. 117–147, 2016.
- [79] H. Gao, C. Birkett, and D. P. Lettenmaier, "Global monitoring of large reservoir storage from satellite remote sensing," *Water Resour. Res.*, vol. 48, no. W09504, pp. 1–12, 2012.
- [80] R. Y. Kuang, W. Luo, and M. Zhang, "Optical classification of Poyang Lake waters based on in situ measurements and remote sensing images," *Resour. Environ. Yangtze Basin*, vol. 24, no. 5, pp. 773–779, 2015.
- [81] A. Getirana, H. C. Jung, and K. H. Tseng, "Deriving 3-D reservoir bathymetry from multi-satellite datasets," *Remote Sens. Environ.*, vol. 217, pp. 366–374, 2018.
- [82] A. Khandelwal, A. Karpatne, M. E. Marlier, J. Kim, D. P. Lettenmaier, and V. Kumar, "An approach for global monitoring of surface water extent variations in reservoirs using MODIS data," *Remote Sens. Environ.*, vol. 202, pp. 113–128, 2017.
- [83] C. Du, S. X. Wang, Y. Zhou, and F. L. Yan, "Impact assessment of cyanobacteria bloom on water intakes in Taihu Lake using remote sensing data," *China Environ. Sci.*, vol. 10, pp. 1041–1046, 2009.
- [84] J. F. Lu, R. H. Xiao, Z. M. Li, X. T. Leng, and D. M. Jie, "The regional difference of type combination of lakes in Songnen Plain," *J. Northeast Normal Univ.*, vol. 2, pp. 99–105, 2000.
- [85] Y. Lu, C. R. Chen, G. H. Liu, and W. Z. Liu, "Sediment nitrogen cycling rates and microbial abundance along a submerged vegetation gradient in a Eutrophic Lake," *Sci. Total Environ.*, vol. 616–617, pp. 899–907, 2018.



**Xiaodi Wang** received the B.S. degree in resource environment, and urban and rural planning the M.S. degree in physical geography and the Ph.D. degree in geography from Harbin Normal University, in 2008, 2010, and 2015, respectively.

She is currently with Harbin University, Harbin, and a Post-doctoral with the Northeast Institute of Geography and Agroecology, Chinese Academy of Sciences, Changchun, China. Her research interests include water environment remote sensing and water environment pollution.



**Kaishan Song** received the M.S. degree in GIS and cartography from Northeast Normal University, Changchun, China in 2002, and the Ph.D. degree in remote sensing application from the Northeast Institute of Geography and Agroecology (IGA), Chinese Academy of Sciences (CAS), Changchun, China, in 2005.

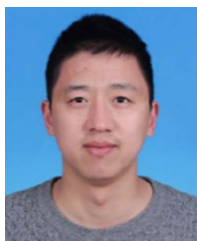
He is currently a Full Professor for remote sensing of environment applications with IGA, CAS. His current research interests include biooptical properties of inland waters, remote sensing of water quality, and impact of climatic and anthropogenic driving forces on water quality spatiotemporal variations with remotely sensed imagery data.



**Zhidan Wen** received the B.S. degree in bioengineering from Northeast Forestry University, Harbin, China, in 2007, the M.S. degree in microbiology from Shenyang Agricultural University, Shenyang, China, in 2010, and the Ph.D. degree in Environmental Science and Engineering from the Harbin Institute of Technology, Harbin, China, in 2014.

She is currently with the Northeast Institute of Geography and Agroecology, Chinese Academy of Sciences, Changchun, China. Her research interests include carbon cycle in water and Greenhouse gas

emissions from inland water bodies.



**Ge Liu** received the B.S. degree in geographical science from Liaocheng University, Liaocheng, China, in 2011 and the Ph.D. degree in environmental remote sensing from Nanjing Normal University, Nanjing, China, in 2017.

He is currently with the Northeast Institute of Geography and Agroecology, Chinese Academy of Sciences, Changchun, China. His research interests include water color remote sensing and optical properties in optically complex water bodies.

**Yingxin Shang** received the B.S. degree in environmental science from the Changchun University of Science and Technology, Changchun, China, in 2012, and the Ph.D. degree in cartography and geographic information system from the University of Chinese Academy of Sciences, Beijing, China, in 2020.

She is currently with the Northeast Institute of Geography and Agroecology, Chinese Academy of Sciences, Changchun, China. Her research interests include water color remote sensing and optical properties in optically complex water bodies.



**Chong Fang** received the B.S. degree in geographical science from Shandong Normal University, Jinan, China, in 2014, the M.S. degree in cartography and geographic information system from the Northeast Institute of Geography and Agroecology, Chinese Academy of Sciences, Changchun, China, and the Ph.D. degree in cartography and geographic information system from Northeast Institute of Geography and Agroecology, Chinese Academy of Sciences, in 2020.

She is currently a Postdoctoral Fellow with the School of Infrastructure Engineering, Dalian University of Technology. Her research interests include remote sensing for water environment.



**Lili Lyu** received the master's degree in inorganic chemistry from the College of Chemistry, Northeast Normal University in 2011. She is currently working toward the Ph.D. degree in cartography and geographic information system at the Northeast Institute of Geography and Agroecology, Chinese Academy of Sciences, Changchun, China.

Her research interests include inversion of water quality parameters, evaluation of water nutritional status, measurement of water optical parameters, data mining, etc.



**Qiang Wang** received the B.S. and M.S. degrees in physical geography from Jilin Normal University, Siping, China, in 2011 and 2019, respectively.

He is currently with the Northeast Institute of Geography and Agroecology, Chinese Academy of Sciences, Changchun, China. His research interests include water color remote sensing and optical properties in optically complex water bodies.